coatings

MDPI

Review

A Review of Carbonation of C-S-H: From Atomic Structure to Macroscopic Behavior

Yi Zhao [1,2] and Junjie Wang [2,*]

[1] Beijing No. 4 Municipal Construction Engineering Co., Ltd., Beijing 100176, China; m13811403000@163.com
[2] Department of Civil Engineering, Central South University, Changsha 410083, China
* Correspondence: junjie-wang@live.cn

Abstract

Calcium–silicate–hydrate (C-S-H), the primary binding phase governing cement paste cohesion, undergoes progressive physicochemical transformation upon carbonation—a process that critically dictates concrete durability in atmospheric environments. When CO_2 penetrates the porous cement matrix, it triggers a cascade of degradation mechanisms: calcium leaching decalcifies the C-S-H structure, inducing polymerization of silicate chains from dimeric to longer-chain configurations, while concurrent precipitation of calcium carbonate and amorphous silica gel fundamentally reconstitutes the nanoscale architecture. These nanoscale alterations propagate to macroscopic property evolution, manifesting as initial strength and stiffness gains due to pore-filling carbonation products followed by eventual deterioration as the cohesive binding network deteriorates. This review synthesizes current understanding of carbonation-induced structural evolution, examining the coupled influences of environmental parameters—CO_2 concentration, relative humidity, and temperature—alongside C-S-H intrinsic chemistry (Ca/Si ratio, aluminum substitution, and alkali content) on reaction kinetics and material performance. However, significant knowledge gaps persist: predictive models for in-service carbonation rates remain elusive due to the disconnect between idealized laboratory conditions and the heterogeneous, cracked reality of field concrete; the causal linkage between nanoscale C-S-H alteration and macroscale cracking patterns along with physical performance is poorly resolved, and most mechanistic studies rely on synthetic C-S-H, neglecting the compositional complexity of real Portland cement systems. We further propose emerging protection strategies, including surface barrier coatings and low-carbon alternative binders (geopolymers, calcium sulfoaluminate cements, carbon-negative materials such as recycled cement), which demonstrate enhanced carbonation resistance. Future research priorities include developing effective coating barriers for carbonation protection, developing operando characterization techniques for real-time reaction monitoring, deploying machine learning algorithms to bridge atomistic simulations with structural-scale predictions, and establishing long-term field performance databases to validate laboratory-derived degradation models.

Keywords: carbonation; C-S-H; microstructure; cement paste; concrete; durability

Academic Editor: Paolo Castaldo

Received: 23 March 2026
Revised: 5 April 2026
Accepted: 7 April 2026
Published: 8 April 2026

1. Introduction

Cement hydration is a complex chemical process that begins when water is added to cement, initiating a series of reactions that ultimately lead to the formation of a solid matrix capable of binding aggregates into a cohesive structure. The primary components of Portland cement, namely tricalcium silicate (C_3S) and dicalcium silicate (C_2S), react with

water to form calcium–silicate–hydrate (C-S-H) and calcium hydroxide ($Ca(OH)_2$). Among these hydration products, C-S-H is the most significant due to its substantial contribution to the strength and durability of cementitious materials. Calcium–silicate–hydrate, commonly referred to as C-S-H, is the primary binding phase in hydrated cement paste. Its formation begins almost immediately after the cement is mixed with water, continuing as the paste cures. C-S-H is an amorphous to poorly crystalline material with a variable stoichiometry, typically represented by the formula $C_3S_2H_3$ (where C = CaO, S = SiO_2, and H = H_2O).

The hydration of cement is an exothermic process where water interacts with the anhydrous cement phases, leading to the formation of hydrated compounds. C-S-H is the principal hydration product of the silicate phases in Portland cement, namely tricalcium silicate (C_3S) and dicalcium silicate (C_2S). The formation of C-S-H is crucial for the development of the cement paste's microstructure and the resultant mechanical properties.

The formation of C-S-H can be represented by the simplified reactions:

$$2(3CaO{\cdot}SiO_2) + 6H_2O \rightarrow 3CaO{\cdot}2SiO_2{\cdot}3H_2O + 3Ca(OH)_2$$

$$2(2CaO{\cdot}SiO_2) + 4H_2O \rightarrow 3CaO{\cdot}2SiO_2{\cdot}3H_2O + Ca(OH)_2$$

Calcium–silicate–hydrate (C-S-H) constitutes the principal binding phase in Portland cement paste, forming through the hydration of tricalcium silicate (C_3S) and dicalcium silicate (C_2S)—the primary alite and belite components of cement clinker. These calcium silicate minerals exhibit markedly different reactivity kinetics: C_3S hydrates rapidly, liberating substantial heat and generating early-age strength within the first 28 days, while C_2S reacts more slowly, contributing progressively to long-term strength development and ultimate durability [1,2]. The C-S-H gel that emerges from these hydration reactions possesses a complex, nanocrystalline to poorly crystalline layered structure that has been conceptualized through several evolving models—from the early tobermorite–jennite structural analogies to the colloidal globule model proposing basic building blocks of approximately 5 nm diameter composed of layered calcium silicate sheets separated by interlayer water. Solid-state ^{29}Si nuclear magnetic resonance spectroscopy reveals that fresh C-S-H predominantly contains Q^1 (end-chain) and Q^2 (middle-chain) silicate tetrahedra organized in linear dreierketten arrangements, with mean chain lengths typically ranging from 2 to 5 tetrahedral units depending on formation conditions. The calcium-to-silicon ratio (Ca/Si) of C-S-H varies considerably, generally falling between 1.2 and 2.0 in ordinary Portland cement pastes, though this ratio can extend lower in systems containing supplementary cementitious materials [3,4]; nanoindentation studies demonstrate that this compositional parameter critically influences mechanical properties, with reduced Ca/Si ratios correlating with increased indentation modulus and hardness due to more extensive silicate polymerization and reduced structural defects. The high specific surface area (50–700 m^2/g depending on measurement method) and substantial interlayer water content—comprising both adsorbed and structural water—endow C-S-H with its characteristic binding capacity, though these same features render the phase vulnerable to environmental degradation, particularly carbonation attack [5,6].

Carbonation of C-S-H proceeds through a well-documented two-step mechanism involving progressive decalcification and structural reorganization rather than instantaneous conversion [7–10]. In the initial stage, calcium ions are leached from interlayer spaces and defect sites within the silicate chains, reducing the Ca/Si ratio to approximately 0.67 while the principal layered structure remains largely intact; ^{29}Si NMR confirms this threshold corresponds to infinite silicate chain configurations where Q^2 units dominate. Upon further carbonation exposure, calcium is extracted from the principal layers themselves, triggering collapse of the layered structure, extensive silicate polymerization toward Q^3 and Q^4

configurations, and ultimate transformation to amorphous silica gel [11–13]. This chemical degradation produces calcium carbonate polymorphs—primarily calcite with transient vaterite and aragonite formation depending on conditions—that precipitate within the pore network, initially reducing porosity and potentially increasing density and mechanical stiffness before eventual strength loss from binding phase decomposition [14,15]. The environmental implications are severe: carbonation drives pore solution pH from the characteristic highly alkaline condition near 12.5–13 to below 9, dissolving the protective passive film (γ-Fe_2O_3) on embedded steel reinforcement and initiating electrochemical corrosion that generates expansive iron oxide products, cracking, and concrete spalling. However, controlled carbonation curing—exposing fresh cement paste or concrete to concentrated CO_2 atmospheres (10%–100% vs. ambient 0.04%)—exploits early-stage densification to achieve rapid strength development, reduced permeability, and permanent CO_2 sequestration within the mineral matrix, offering a sustainable manufacturing alternative that can achieve carbonation efficiency and compressive strength improvements compared to conventional water curing.

Recent research has increasingly focused on elucidating carbonation mechanisms at atomic and nanoscale resolutions to enable predictive modeling and engineered material design [16–21]. Advanced characterization techniques including in situ synchrotron X-ray diffraction, cryo-transmission electron microscopy, and small-angle neutron scattering have revealed that C-S-H formation proceeds through metastable precursor phases that subsequently crystallize to tobermorite-type structures, while carbonation induces continuous rather than stepwise structural evolution. Molecular dynamics simulations and force-field calculations have established quantitative relationships between C-S-H nanostructure and mechanical properties, demonstrating that interlayer water and calcium coordination environments govern creep behavior and elastic anisotropy. Critical knowledge gaps persist, however: real-time tracking of silica gel structural evolution during carbonation remains experimentally challenging, the polymorphic transition sequence from amorphous calcium carbonate through vaterite to calcite in confined nanoscale pores lacks quantitative description, and standardized methods to predict service-life carbonation depths from short-term laboratory data remain elusive. Future progress will require integrating multiscale characterization with machine learning-assisted predictive modeling, developing novel admixtures that guide carbonate crystallization toward beneficial morphologies, and establishing rigorous long-term validation protocols that connect laboratory findings to field performance across diverse environmental exposures.

This review aims to provide a comprehensive understanding of the carbonation process, its effects on C-S-H, and the implications for the durability of cement-based materials. Emphasis is placed on three interconnected aspects: (1) atomic-level restructuring of silicate tetrahedra and calcium coordination environments; (2) microstructural evolution encompassing morphology, porosity, and phase distribution; and (3) compositional shifts involving Ca/Si ratio reduction and carbonate polymorph formation. This review provides a comprehensive framework for understanding carbonation of C-S-H.

2. C-S-H Phase in Cement Paste

2.1. Composition and Structure of C-S-H

Calcium–silicate–hydrate (C-S-H) possesses a structurally complex, nanocrystalline to poorly crystalline layered architecture built from fundamental silicate tetrahedra (SiO_4^{4-}) that polymerize through bridging oxygen atoms to form linear or branched chain structures. These silicate chains are separated by interlayer calcium polyhedra that serve as the primary structural glue, while substantial quantities of interlayer and gel water occupy the intralamellar spaces and nanopores, collectively generating the high specific surface

area and nanoporosity that govern C-S-H's physicochemical behavior [8]. At the nanoscale, this disordered arrangement of silicate chains, calcium cations, and water molecules creates a gel-like material whose exact structural order remains challenging to characterize precisely. Morphologically, C-S-H exhibits considerable diversity across length scales, manifesting as fibrous, foliated, reticulated, or granular textures depending critically on formation conditions—particularly water-to-cement ratio, curing temperature, and hydration age—which in turn influence packing density and interfacial bonding characteristics. These structural attributes collectively establish C-S-H as the principal binding phase in hardened cement paste, conferring mechanical integrity through its high surface area and nanoscale confinement effects while simultaneously dominating time-dependent phenomena including drying shrinkage, creep deformation, and transport properties such as permeability that ultimately determine concrete durability.

C-S-H has a variable Ca/Si ratio (Figure 1). It typically spans 1.2 to 2.0 or 0.5 to 0.8 for the Si/Ca ratio. The exact value depends on hydration conditions and cement chemistry. This ratio controls density and porosity. Low ratios give open, porous structures. More silicate tetrahedra appear. High ratios produce denser microstructures. Porosity drops. Durability and performance shift accordingly.

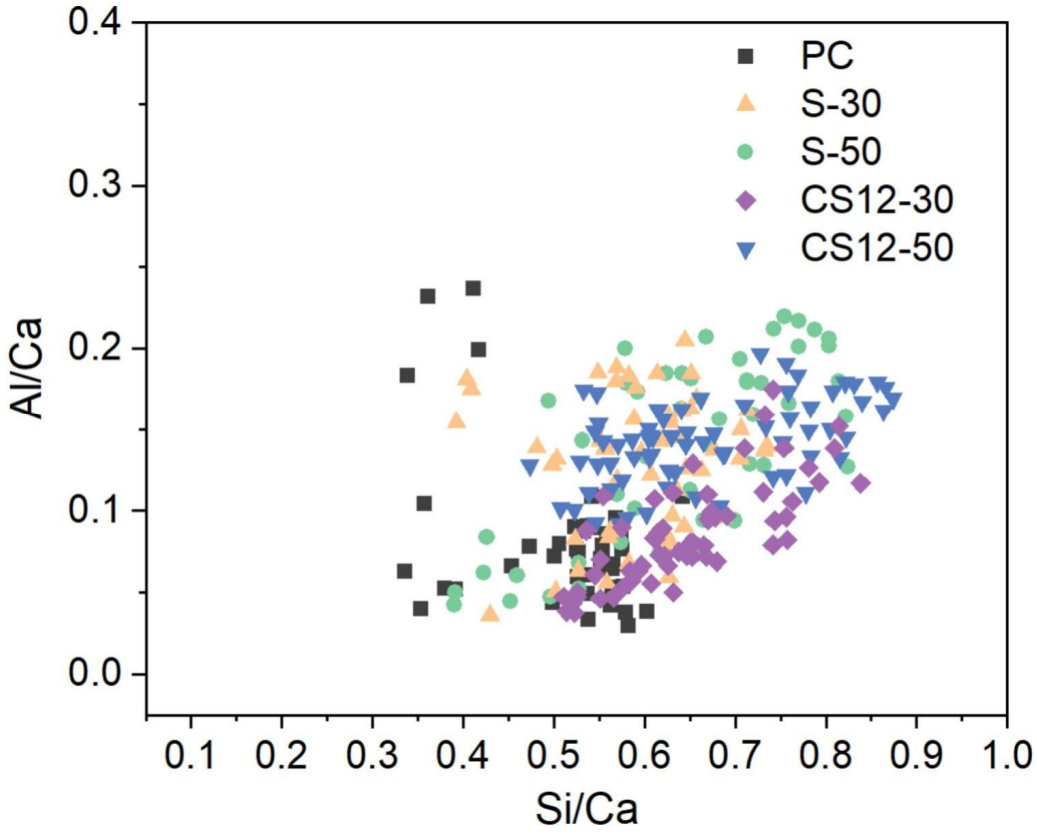

Figure 1. Al/Ca versus Si/Ca atomic ratios on C-(A)-S-H for cement pastes with different additives at 28 days [1].

2.2. Properties and Role of C-S-H in Cement Paste

C-S-H and other phases (Figure 2) govern most mechanical properties of hardened paste. Different additives caused different compositions in the cement paste, as shown in Figure 2. Its gel structure supplies cohesion and strength. Its nanoporosity controls permeability and durability. The C/S ratio of C-S-H varies. It normally sits between 1.2 and 2.0. This ratio affects stability and reactivity. High ratios mean high alkalinity. Yet they also mean lower durability when conditions turn aggressive. Carbonation is one such threat.

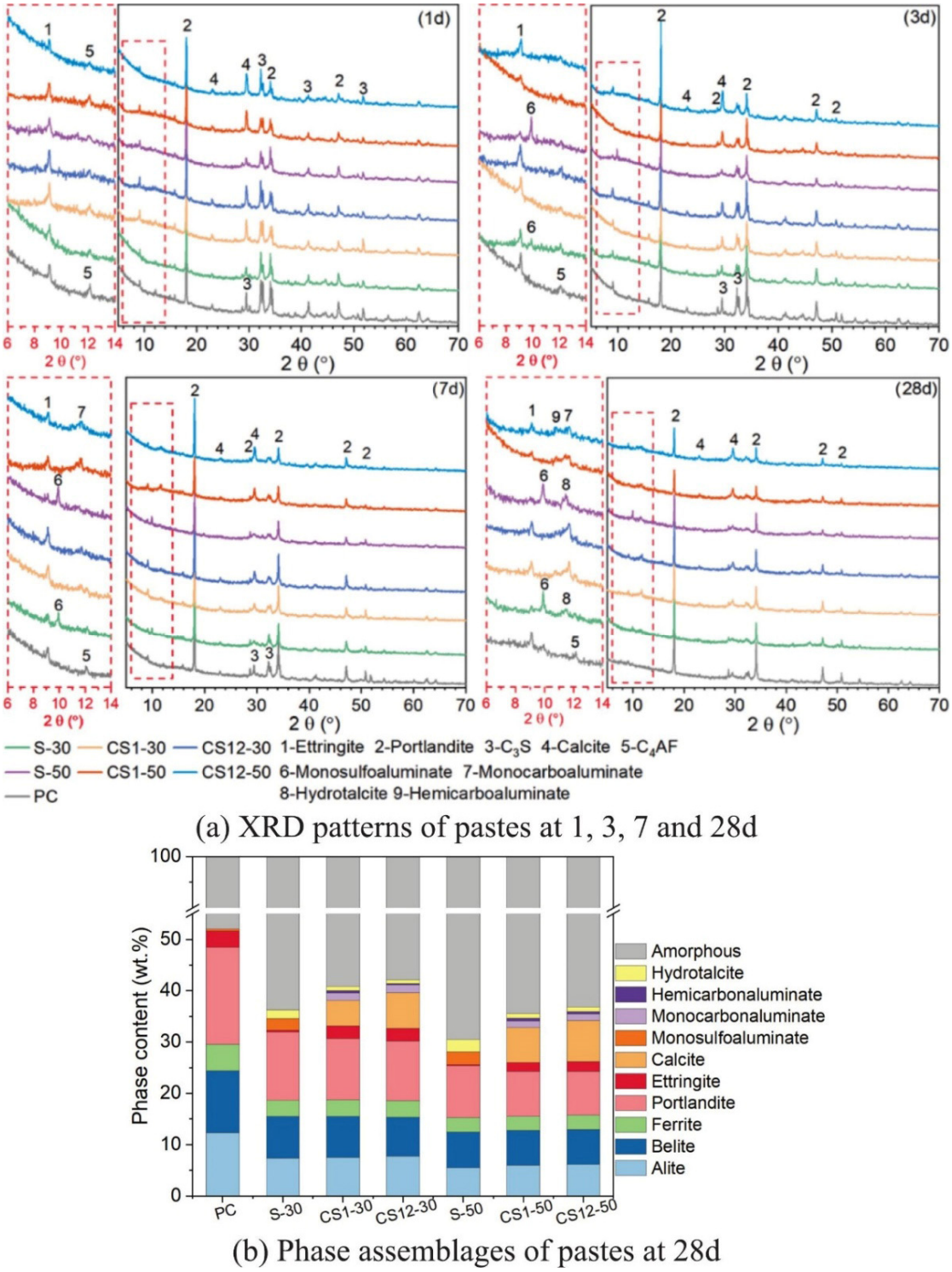

Figure 2. XRD patterns and QXRD results of cement pastes with different additives [1].

C-S-H governs compressive strength and elasticity. These properties shape how cement paste performs. Its high surface area and nanoporosity create strong capillary forces. These forces add to material strength. Yet these same traits expose C-S-H to environmental attack. Carbonation is the main concern. Chemically, C-S-H stays stable in alkaline pore solutions. Acidic conditions trigger change. Carbonation does too. Calcium leaves the structure. This is decalcification. Binding capacity drops. Porosity rises. Cement paste durability suffers.

3. Mechanism of Carbonation in Cement Paste

3.1. Chemistry of Carbonation Reaction

Carbonation represents a complex, multi-stage reaction process in which atmospheric CO_2 penetrates the porous cement matrix and attacks calcium-bearing phases, ultimately precipitating calcium carbonate (Figure 3). In the case of C-S-H—where the reaction mechanism is particularly intricate—carbonation proceeds through coupled dissolution-precipitation and ion-exchange phenomena. Initially, carbonic acid formed from CO_2 dissolution dissociates to release hydrogen ions that penetrate the C-S-H interlayer regions, displacing calcium through an ion-exchange mechanism where Ca^{2+} leaches from the structure and protons occupy the vacated coordination sites, thereby progressively decalcifying the calcium–silicate framework. Simultaneously, the liberated calcium ions migrate through the pore solution toward regions of higher CO_2 concentration, where they react with carbonate ions to nucleate and grow $CaCO_3$, typically precipitating within available pore spaces and on exposed surfaces. This decalcification-precipitation coupling fundamentally alters the C-S-H stoichiometry and nanostructure: as calcium is stripped from the interlayer calcium polyhedra, the silicate chains undergo condensation and polymerization, transforming the original tobermorite-like structure into a progressively silica-rich, less cross-linked gel while the precipitated carbonate phase fills porosity and modifies the microstructural topology.

$$Ca(OH)_2 + CO_2 \rightarrow CaCO_3 + H_2O$$

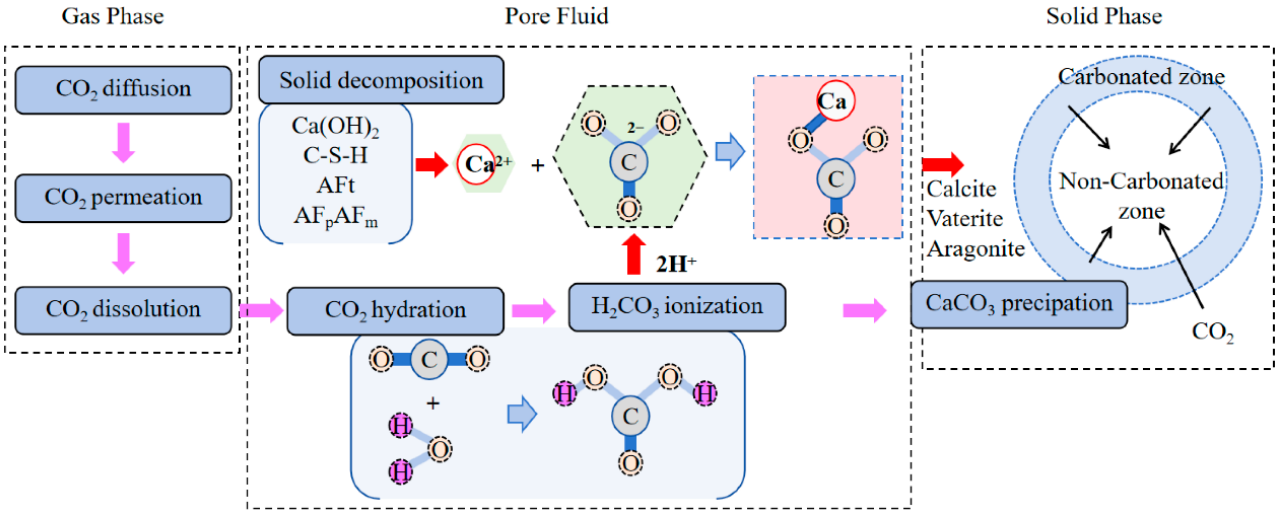

Figure 3. Carbonation reaction in cement paste [16].

Carbonation proceeds via progressive decalcification of the C-S-H structure, yielding two distinct reaction products: calcium carbonate precipitates within the pore network and at exposed surfaces, while amorphous silica gel ($SiO_2 \cdot nH_2O$) remains as a residual solid phase [9]. This transformative process generates competing microstructural effects—while $CaCO_3$ crystallization fills capillary pores and increases local density, the concomitant release of calcium ions and proton intrusion causes a sharp decline in pore solution pH that compromises the passivating environment essential for steel reinforcement durability [10–13]. The reaction front advances through a diffusion-controlled mechanism wherein CO_2 penetrates the tortuous pore structure of the hardened paste [14], with propagation rates governed by the interplay of environmental parameters including atmospheric CO_2 concentration, relative humidity, temperature, and the intrinsic

permeability of the cementitious matrix [15]. Unlike the simplified stoichiometric representation often depicted as

$$\text{C-S-H} + CO_2 \rightarrow CaCO_3 + SiO_2 \cdot nH_2O$$

Carbonation is in reality a continuous, multi-step process characterized by gradual Ca/Si ratio reduction rather than instantaneous conversion. As decalcification progresses, C-S-H evolves through a series of metastable states—transforming from a calcium-rich, tobermorite-like gel to progressively silica-rich, disordered structures with shortened silicate chain lengths and altered mechanical properties [22], thereby precluding any single-step chemical equation from adequately capturing the reaction's kinetic complexity or structural nuance.

3.2. Distinctions Between Carbonation of Different Phases

The carbonation susceptibility and reaction mechanisms differ markedly among the principal calcium-bearing phases in hydrated cement paste, with portlandite (CH), ettringite (AFt), monosulfate (AFm), and C-S-H each exhibiting distinct chemical pathways and kinetic profiles. Portlandite carbonation proceeds most readily due to its high calcium content, simple crystal structure, and favorable solubility, undergoing a straightforward acid-base reaction where CO_2 reacts directly with $Ca(OH)_2$ to precipitate calcite while consuming acidity and buffering the pore solution pH; this rapid consumption of CH depletes the alkaline reserve that otherwise protects embedded steel, making portlandite carbonation particularly consequential for reinforcement corrosion initiation. In contrast, AFt and AFm phases—alumina-ferric oxide tri- and monosulfate hydrates, respectively—present more complex carbonation chemistries governed by their layered structures and variable anion exchange capacities; AFt carbonation typically involves sulfate substitution by carbonate to form thaumasite or ettringite-derived carbonate phases under favorable conditions, while AFm transforms through sequential anion exchange and structural rearrangement into hemicarbonate or monocarbonate forms, with both conversions potentially releasing sulfate ions that may subsequently react with remaining aluminate phases or participate in delayed ettringite formation depending on environmental moisture and temperature regimes.

These phase-specific carbonation pathways generate divergent microstructural consequences that propagate to distinct durability implications across the cement matrix. Portlandite carbonation produces expansive calcite crystallization that can temporarily densify the paste and reduce permeability, yet this benefit is offset by the complete removal of a pH-buffering phase and the creation of shrinkage-prone silica-rich regions where CH previously resided. C-S-H carbonation, as detailed previously, induces progressive decalcification and silicate polymerization that initially strengthens through pore-filling precipitation but ultimately weakens the binding gel structure, whereas AFt and AFm carbonation introduce additional chemical complexity through aluminum redistribution and potential secondary mineral formation that may either consolidate or disrupt the microstructure depending on the balance between carbonate incorporation and sulfate release. The relative rates of these concurrent carbonation reactions establish a competitive hierarchy—portlandite typically reacts first and fastest, followed by AFm and AFt phases, with C-S-H carbonation proceeding more gradually but persisting longer due to its abundance and kinetic hindrance imposed by its nanostructured, poorly crystalline nature.

Understanding these interphase distinctions proves essential for predictive modeling and durability engineering, as the overall carbonation depth and damage progression in concrete emerge from coupled, non-simultaneous reactions rather than single-phase behavior. In blended cements where supplementary cementitious materials reduce portlandite

content, C-S-H and AFm carbonation assume greater relative importance, potentially accelerating degradation rates despite slower intrinsic kinetics due to diminished alkaline buffering capacity. Similarly, sulfate exposure environments may suppress AFt carbonation through competitive stabilization, while carbonation-induced AFm transformation can influence subsequent chloride binding capacity and thus alter corrosion risk profiles in marine or de-icing salt applications.

3.3. Factors Affecting Carbonation

3.3.1. Environmental Factors

Carbonation kinetics are governed by the coupled influence of CO_2 concentration, relative humidity, and temperature, each imposing distinct quantitative constraints and mechanistic controls on reaction rate through their effects on gas transport, aqueous dissolution, and chemical activation. CO_2 concentration establishes the fundamental thermodynamic driving force: carbonation depth typically scales with the square root of CO_2 partial pressure under diffusion-controlled conditions, with laboratory studies demonstrating that elevating concentration from ambient ~400 ppm to 1%–3% accelerates rates by one to two orders of magnitude, while industrial carbonation curing employs 10%–100% CO_2 to achieve completion within hours [17,21,23]. Relative humidity exerts a non-monotonic, parabolic influence with maximum rates observed at 50%–70% RH—below ~40% insufficient water film thickness impedes CO_2 dissolution and ionic mobility, while above ~85% capillary condensation blocks gas-phase diffusion through pore networks, reducing effective permeability by orders of magnitude and shifting control to slow liquid-phase CO_2 transport [18,24]. Temperature accelerates carbonation through competing pathways: Arrhenius-type rate constants for chemical reaction typically double per 10 °C increase between 20 and 60 °C (activation energy ~40–60 kJ/mol for decalcification), yet simultaneous microstructural coarsening of C-S-H at elevated curing temperatures reduces specific surface area and reactive calcium accessibility, potentially offsetting kinetic gains in field exposures where thermal history varies [19,20,25]. The interplay of these factors produces environment-specific rate laws: carbonation depth evolution follows parabolic time dependence ($x = K\sqrt{t}$) under diffusion-dominated ambient conditions where K incorporates pCO_2 and temperature-dependent diffusivity, whereas accelerated carbonation curing operates under chemically controlled linear kinetics until product layer densification re-establishes diffusion limitation.

The rate-controlling mechanism of carbonation shifts between diffusion limitation and reaction kinetic control depending critically on environmental conditions, material microstructure, and reaction progression, with most practical scenarios exhibiting coupled behavior rather than pure single-mechanism dominance. Under conditions of high CO_2 concentration, low relative humidity, or within dense, low-permeability cement pastes, CO_2 transport through the pore network becomes sufficiently restricted that diffusion emerges as the primary rate-limiting step, causing carbonation to proceed via a sharp, advancing reaction front where fully carbonated material overlies uncarbonated paste with minimal intermediate transition zone. Conversely, at elevated humidity levels where pore saturation impedes gas-phase CO_2 diffusion, or in highly porous systems with abundant reactive calcium phases, the intrinsic chemical reactivity of decalcification and carbonate nucleation becomes rate-determining, resulting in distributed, gradual carbonation throughout the material thickness rather than sharp front propagation. Temperature exerts a dual influence—accelerating both diffusion coefficients and reaction rates—yet the activation energies differ between transport and chemical processes, causing the dominant mechanism to vary seasonally or geographically even for identical concrete compositions. Most realistically, carbonation operates under mixed control where CO_2 diffusion through the

carbonated layer slows progressively as $CaCO_3$ precipitation densifies this zone, while the underlying reaction kinetics simultaneously decelerate due to C-S-H decalcification and reduced calcium availability, producing the characteristic parabolic or power-law carbonation depth evolution observed in field exposures. This mechanistic duality complicates predictive modeling, as simplified diffusion-based service life models may overestimate performance when reaction kinetics dominate—particularly for blended cements with slower-reacting slag or fly ash phases—while purely kinetic approaches fail to capture the protective effects of carbonation-induced densification that temporarily retard further CO_2 ingress.

3.3.2. Material Properties

The kinetics and extent of carbonation are governed by the microstructural architecture of the cement paste, particularly porosity and pore connectivity, which control CO_2 diffusion pathways and reactive surface area availability. Higher total porosity—whether arising from elevated water-to-cement ratios, inadequate curing, or inherent phase packing characteristics—reduces tortuosity and increases the effective diffusion coefficient of CO_2 through the pore network, directly accelerating carbonation front propagation according to Fick's laws of diffusion [26]. The specific surface area and polymerization degree of C-S-H further influence reactivity: fresh, high-surface-area C-S-H with extensive Q^1 and Q^2 chain termini presents more reactive calcium sites and silanol groups for carbonate nucleation compared to aged, polymerized material with longer chain lengths and reduced surface area [26–28]. Paste composition critically shapes these microstructural parameters, with water-to-cement ratio serving as the dominant mixing variable that controls initial capillary porosity and subsequent hydration product density. Supplementary cementitious materials (SCMs) such as fly ash and ground granulated blast-furnace slag introduce additional complexity: by consuming portlandite through pozzolanic reactions and producing additional C-S-H with refined pore structure, SCMs typically reduce total $Ca(OH)_2$ content and decrease mean pore diameter, thereby lowering carbonation rates despite increasing total C-S-H surface area [29–31]. However, this protective effect depends on curing quality and SCM replacement level—insufficient curing or high-volume SCM substitution can leave residual capillary porosity that outweighs microstructural refinement, potentially increasing rather than decreasing carbonation susceptibility in field exposures where moisture and temperature fluctuate.

4. Effects of Carbonation on C-S-H and Cement Paste

4.1. Atomic-Scale Structural Changes of C-S-H Due to Carbonation

Carbonation induces progressive structural reorganization of the C-S-H silicate framework through coupled decalcification and polymerization reactions that transform the material from a ductile, ionically bonded gel to a rigid, covalently crosslinked silica-rich product. Fresh C-S-H predominantly contains Q^1 (end-chain) and Q^2 (middle-chain) silicate tetrahedra arranged in short dreierketten configurations, with mean chain lengths typically ranging from 2 to 5 tetrahedral units depending on formation conditions and Ca/Si ratio. As shown in Figures 4 and 5, the molar volume and mean chain length of C-S-H both change with changing Ca/Si ratios. Decreasing Ca/Si ratio causes decreasing molar volume of C-S-H but increasing mean chain length. Upon CO_2 exposure, the initial decalcification stage—characterized by leaching of weakly bound interlayer Ca^{2+} that maintains pH above 13—promotes silicate chain condensation as Q^1 end-units link to form additional Q^2 middle-units, extending mean chain lengths while preserving the overall layered structure [32]. This early polymerization occurs without significant structural collapse because the principal-layer calcium ions that stabilize the silicate sheets remain in place;

however, once decalcification progresses sufficiently to drive Ca/Si below approximately 0.78, calcium extraction from the main layers triggers dissolution of the chain structures and framework destabilization [33]. During this advanced stage, as pH falls below 11, further condensation generates Q^3 (cross-linked branching) and Q^4 (fully condensed three-dimensional network) species that signal transformation toward amorphous silica gel, with ^{29}Si NMR confirming the emergence of Q^3/Ca and Q^3/Q^4 environments alongside the steady decline in Q^1/Q^2 ratio as carbonation advances [34]. Sodium and potassium ions may transiently substitute for calcium in the interlayer spaces during this transition, providing temporary structural stabilization that delays but cannot ultimately prevent complete framework collapse upon continued CO_2 attack. These chemical transformations fundamentally alter the bonding character throughout the material: the ionic Si–O–Ca linkages that impart ductility and toughness in fresh C-S-H progressively convert to more covalent Si–O–Si bonds that increase rigidity while reducing fracture resistance, explaining the observed mechanical embrittlement and loss of cohesive energy that accompany advanced carbonation in cementitious systems.

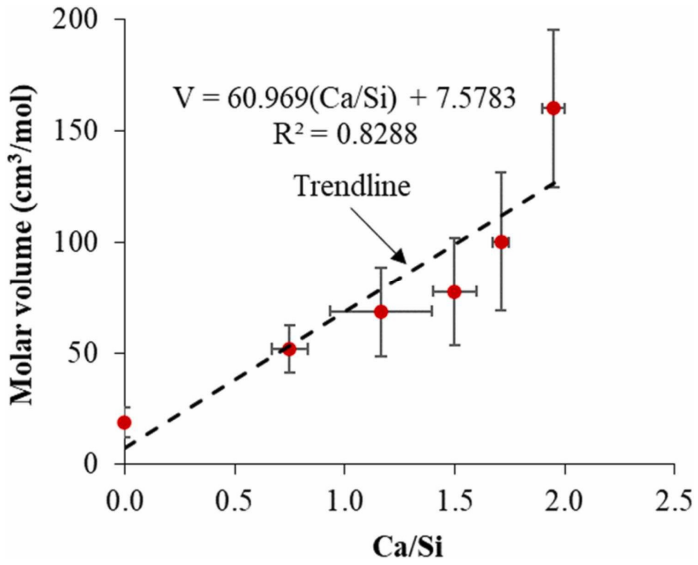

Figure 4. Molar volume of C-S-H vs. Ca/Si [35].

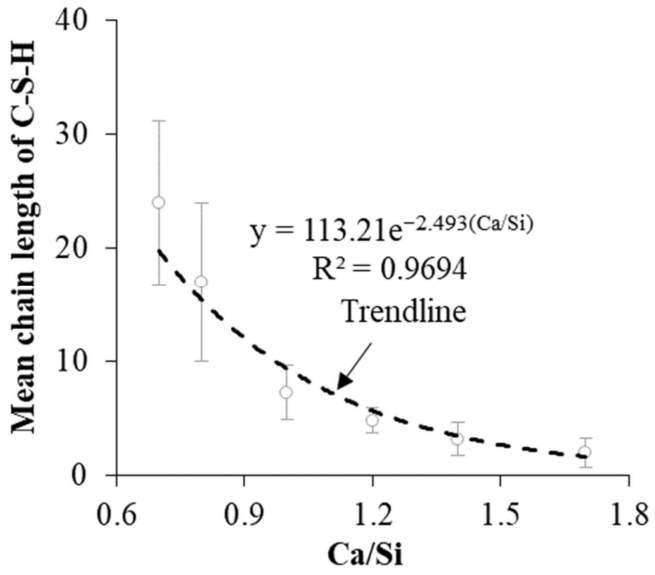

Figure 5. Mean chain length of C-S-H vs. Ca/Si [35].

4.2. Microstructural Changes of C-S-H Due to Carbonation

Initially, fresh C-S-H exhibits a foil-like or sheet-like morphology and is nanocrystalline in nature. As carbonation proceeds, the extraction of calcium ions from the C-S-H structure drives a reduction in the interlayer spacing, leading to macroscopic contraction of the material. This contraction generates internal tensile stresses, which ultimately manifest as microcracks (Figure 6). Concurrently, the liberated calcium reacts with carbonate species to precipitate $CaCO_3$ crystals, predominantly in the form of calcite or aragonite. These crystals nucleate and grow, but often detach from the surrounding C-S-H matrix due to differential volume changes and poor interfacial adhesion, resulting in a clear phase separation. The departure of Ca^{2+} also promotes the polymerization of silicate chains, while the formation of both silica gel and $CaCO_3$ alters the pore network. Specifically, the pore structure coarsens, and the specific surface area declines [36]. Over time, the original crystallinity of the C-S-H fades, and even the newly formed $CaCO_3$ appears as nanocrystals; with continued carbonation, the entire microstructure eventually becomes largely amorphous [37]. This deep decalcification fundamentally reshapes the C-S-H microstructure, reducing the calcium-to-silicon (C/S) ratio, modifying the morphology and connectivity of the silicate chains [38–40]. Notably, the overall porosity can either increase or decrease depending on the balance between calcium leaching and pore filling: when precipitated $CaCO_3$ fails to fill all the voids left by the dissolved calcium, porosity rises [35,41]. Thus, carbonation does not merely alter the phase assemblage but drives a cascade of coupled chemo-mechanical changes that dictate the long-term transport and mechanical behavior of the cementitious matrix. Calcium carbonate precipitates play a pivotal, dualistic role in microstructural evolution during carbonation, simultaneously densifying and destabilizing the cementitious matrix depending on precipitation location, polymorph, and crystallization dynamics. Initially, $CaCO_3$ nucleation within capillary pores and at air-paste interfaces generates pore-filling crystallization that reduces total porosity, increases bulk density, and temporarily enhances mechanical stiffness through load-bearing solid formation; however, this apparent consolidation masks underlying structural degradation, as the same precipitation process depletes calcium from C-S-H and CH phases, compromising the cohesive binding network that governs long-term strength and fracture resistance. The polymorphic diversity of precipitated carbonate—vaterite, aragonite, and calcite—further complicates microstructural outcomes, with metastable vaterite and aragonite eventually transforming to stable calcite through Ostwald ripening, generating crystallization pressures that may induce microcracking and permeability increases that counteract initial densification benefits. Moreover, $CaCO_3$ precipitation at the carbonation front creates a partially obstructive barrier that slows subsequent CO_2 ingress through the reacted layer, establishing a self-limiting kinetic regime where reaction rates become diffusion-controlled through the carbonated zone; this protective effect proves transient, however, as differential crystallization stresses, continued decalcification of residual C-S-H, and pH decline eventually propagate microcracks that re-establish transport pathways and accelerate degradation. Ultimately, the net microstructural impact of $CaCO_3$ formation hinges on the competition between physical pore blocking—which temporarily improves barrier properties—and chemical destabilization of the binding phases, with the balance shifting toward net deterioration as carbonation progresses and the silica-rich residual gel loses structural integrity.

Carbonation-induced shrinkage constitutes a critical, often overlooked degradation mechanism that arises from the coupled physicochemical transformations occurring within the cement paste microstructure during CO_2 exposure. The primary driver is the loss of structurally bound water from the C-S-H interlayer regions as calcium leaching and silicate polymerization proceed: decalcification reduces the charge-balancing requirement for water

molecules coordinating calcium ions, while simultaneously increasing surface silanol group density promotes condensation reactions that expel water during siloxane bond formation. This chemically driven water release—distinct from drying shrinkage—generates capillary tension within the increasingly tortuous, partially emptied pore network, producing substantial volumetric contraction that can exceed 1000 microstrain in fully carbonated pastes. The magnitude of carbonation shrinkage scales inversely with initial Ca/Si ratio and directly with the extent of decalcification, explaining why blended cements with lower portlandite reserves often exhibit more severe dimensional instability despite their generally superior carbonation resistance. When constrained by reinforcement, aggregate interlock, or differential carbonation gradients through the concrete section, this shrinkage translates into tensile stress accumulation that frequently exceeds the reduced tensile capacity of carbonated material, initiating microcracking perpendicular to the exposed surface. These cracks propagate preferentially through the weakened, decalcified C-S-H matrix and at aggregate-paste interfaces, creating interconnected transport pathways that dramatically increase gas permeability and oxygen diffusivity—paradoxically accelerating both further carbonation penetration and, in reinforced elements, corrosion initiation by short-circuiting the protective cover. The resulting crack network also compromises load-bearing capacity through elastic modulus reduction and stress concentration, establishing carbonation shrinkage as a primary mechanistic link between nanoscale chemical alteration and macroscopic structural deterioration that service life models must incorporate to avoid non-conservative durability predictions.

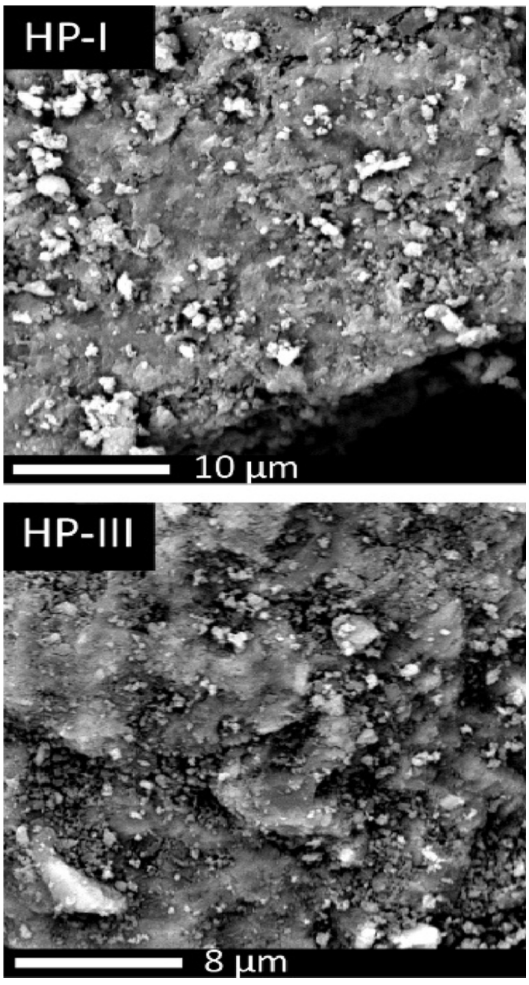

Figure 6. Morphology of hydrated cement paste before (**above**) and after carbonation (**below**) [19].

The distribution, quantity, and crystalline form of calcium carbonate precipitated during carbonation depend sensitively on environmental conditions, paste chemistry, and reaction kinetics, with three polymorphs typically identified in carbonated cement systems: thermodynamically stable calcite (trigonal), metastable aragonite (orthorhombic), and vaterite (hexagonal) [42]. CO_2 concentration exerts primary control over polymorph selection: high CO_2 partial pressures favor calcite formation through accelerated nucleation and growth rates, while intermediate concentrations and temperatures may stabilize aragonite or vaterite, particularly in the presence of magnesium or other impurities that disrupt calcite lattice incorporation [42]. Temperature further influences polymorphism, with elevated curing temperatures generally promoting calcite and higher crystallinity, whereas rapid carbonation at ambient or reduced temperatures tends to preserve metastable forms or generate poorly crystalline phases. These carbonate precipitates occupy distinct microstructural locations—filling capillary pores, coating C-S-H surfaces, and replacing portlandite crystals—with their spatial distribution determining mechanical consequences. Pore-filling calcite can increase matrix density and elastic modulus through solid volume expansion and load-bearing capacity, yet non-uniform crystallization generates localized stress concentrations at interfaces between expanding carbonate and shrinking, decalcified C-S-H, potentially initiating microcracking that compromises long-term integrity despite apparent early-stage densification [42].

4.3. Composition Changes of C-S-H Due to Carbonation

Fresh C-S-H typically starts with Ca/Si between 1.2 and 1.7. This ratio drops steadily as carbonation proceeds. Even after prolonged exposure, residual C-S-H with Ca/Si around 0.60 may remain. At the onset of carbonation, C-S-H and $CaCO_3$ coexist. Once carbonation finishes, only $CaCO_3$, silica gel, and possibly some residual C-S-H remain. Active decalcification releases silicate monomers into solution. When pH falls low enough, these reprecipitate as amorphous, highly polymerized SiO_2 gel. The $CaCO_3$ polymorphs transform in stages. ACC converts to vaterite, then to calcite. This happens through dissolution and recrystallization (Figure 7). All three forms may appear together at intermediate stages. Silicate ions in solution stabilize ACC. They also slow calcite formation. This explains why pure C-S-H carbonation yields more persistent vaterite than carbonation of bulk cement paste.

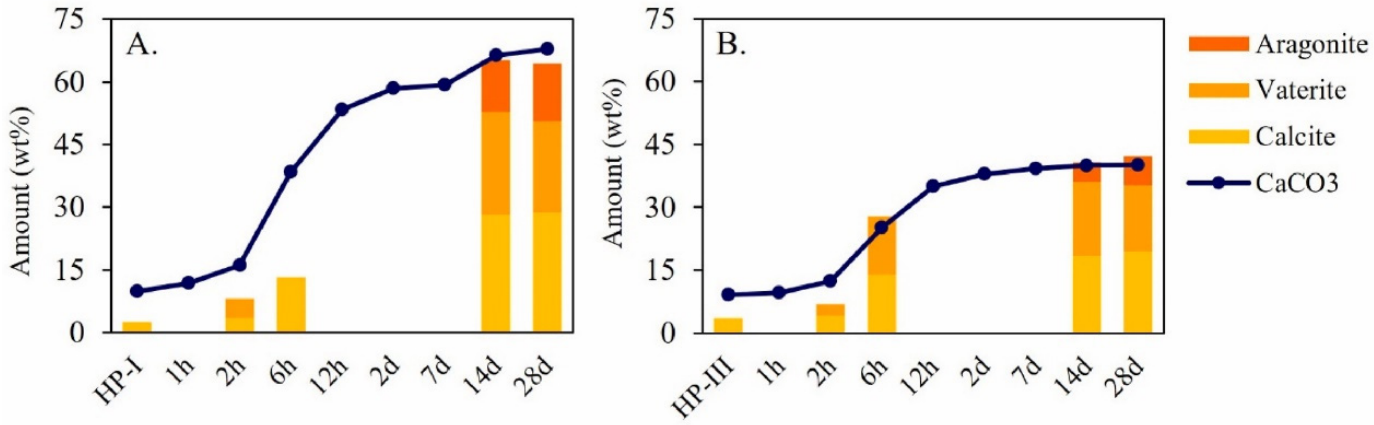

Figure 7. Amount of different forms of $CaCO_3$ with increasing carbonation time ((**A**): HP-I sample with OPC cement, (**B**): HP-III sample with 30% OPC + 70% blast furnace slag) [19].

4.4. Impact on Mechanical Properties of Cement Paste

Carbonation exerts profound, temporally divergent effects on the mechanical performance and durability of cementitious systems, manifesting initially as apparent property

enhancement through microstructural densification before yielding progressive deterioration as chemical degradation advances. During early carbonation stages, $CaCO_3$ precipitation within accessible pore space increases solid volume fraction and reduces total porosity, producing measurable gains in compressive strength and elastic modulus as the crystalline carbonate phase contributes load-bearing capacity and stiffens the composite microstructure [43–45]. However, continued CO_2 exposure initiates a damaging transition: sustained C-S-H decalcification strips calcium from the binding gel structure, reducing cross-linking density and cohesive integrity, while simultaneous pore solution pH decline—from the characteristic highly alkaline condition near 12.5 to values below 9—fundamentally compromises the passivating environment that maintains steel reinforcement durability [46]. This pH reduction proves particularly consequential because the protective γ-Fe_2O_3 layer that naturally forms and stabilizes on embedded steel surfaces dissolves thermodynamically once pH falls below approximately 11, exposing bare metal to oxygen and moisture ingress; with the passive film destroyed, electrochemical corrosion initiates rapidly, generating expansive iron oxide products that generate tensile stresses exceeding concrete capacity, propagating cracks that accelerate both carbonation front penetration and further corrosion in a self-reinforcing degradation cycle culminating in concrete spalling and structural cross-section loss.

Carbonation curing deliberately exploits early-stage densification phenomena while circumventing later deterioration through controlled process design, offering a sustainable manufacturing alternative to conventional hydration-dominated curing [47,48]. In this accelerated approach, fresh or pre-conditioned cement paste or concrete undergoes exposure to concentrated CO_2 atmospheres—typically 10%–100% concentration versus ambient 0.04%—promoting rapid chemical reaction between CO_2 and available calcium phases, predominantly portlandite and superficial C-S-H layers, to precipitate nanocrystalline $CaCO_3$ and polymerized silica gel throughout the pore network within hours rather than the weeks required for conventional hydration [49]. The resulting microstructure exhibits dramatically refined pore size distribution, substantially reduced permeability [50,51], and enhanced early-age strength that facilitates accelerated demolding and construction scheduling, while simultaneously achieving permanent CO_2 sequestration within the mineral matrix that advances carbon utilization objectives without compromising—and often improving—long-term durability performance [16,52–54].

5. Mitigation Strategies for Carbonation

Supplementary cementitious materials (SCMs) including fly ash, ground granulated blast-furnace slag, and silica fume provide substantial protection against carbonation through multiple, synergistic mechanisms that modify both the chemical composition and microstructural characteristics of the hardened paste [55,56]. By reacting with calcium hydroxide through pozzolanic reactions, SCMs consume the primary carbonation-susceptible phase while generating additional C-S-H that refines pore structure, reduces total porosity, and decreases mean pore diameter—typically shifting the pore size distribution toward finer gel pores that impede CO_2 diffusion despite increasing total C-S-H surface area [57,58]. The effectiveness of SCM protection depends critically on curing conditions: adequate humidity (>95% relative humidity) and temperature (20–25 °C) during early hydration ensure complete pozzolanic reaction and dense microstructure formation, whereas poor curing leaves residual capillary porosity that can actually increase carbonation susceptibility despite reduced $Ca(OH)_2$ content [59,60]. Others, like carbon-negative materials such as recycled cement [59] and other carbon sequestration materials, could be useful for preventing carbonation-induced deterioration.

Beyond material modification, surface treatments including penetrating sealers, effective coatings, and membranes provide physical barriers that directly block CO_2 ingress; acrylic, epoxy, and polyurethane coatings can reduce carbonation rates by orders of magnitude when properly applied to sound concrete surfaces, though their long-term effectiveness depends on adhesion quality, UV stability, and resistance to mechanical damage that could compromise barrier continuity [61].

6. Future Research Directions

Future work should push advanced characterization tools for deeper insight into C-S-H carbonation. In situ X-ray diffraction tracks phase changes as they happen. Synchrotron methods reveal atomic-scale structure with high resolution. Atomic force microscopy maps surface transformations in real time. These tools can capture dynamic processes that conventional methods miss. Computational modeling needs further refinement to predict long-term C-S-H behavior across environments. Current models struggle with scale bridging. Nanoscale reaction kinetics do not translate easily to macroscopic performance. Machine learning may help connect these scales. Better models would guide the design of more durable materials by clarifying carbonation kinetics at both micro- and macro-levels. Sustainable cementitious materials demand continued attention. Low-carbon cements and alternative binders are essential for cutting concrete's environmental footprint. These materials must resist carbonation without sacrificing mechanical performance or durability. A critical bottleneck remains: most alternative binders show higher intrinsic porosity or lower alkalinity, making them paradoxically more vulnerable to the very process they aim to mitigate. Balancing carbon footprint with carbonation resistance is an unresolved challenge. Several gaps still block progress. Real-time tracking of silica gel evolution during carbonation remains difficult. The transition from amorphous to crystalline $CaCO_3$ in confined pore spaces is poorly understood. Long-term field data linking laboratory findings to actual structural performance is scarce. Without this validation, predictive models stay theoretical.

7. Conclusions

This work provides a detailed review of the carbonation of C-S-H from atomic structure to macroscopic behavior, and the following conclusions can be made:

1. This review has examined the carbonation processes in C-S-H that influence the long-term performance of cementitious materials. The mechanism proceeds through distinguishable stages: initially, calcium leaves interlayer spaces and chain defect sites, reducing the Ca/Si ratio to approximately 0.67 while the silicate framework remains relatively intact; subsequently, further calcium loss from principal layers leads to structural collapse, silicate chain destabilization, and polymerization toward amorphous silica gel with increased Q^3 and Q^4 site populations. Characterization studies have shown how incongruent dissolution, silicate polymerization, and carbonate crystallization kinetics collectively modify microstructure, with these nanoscale changes correlating with measurable shifts in engineering properties including strength evolution, permeability reduction, and altered durability characteristics. Carbonation thus represents a chemically complex phenomenon with significant practical implications for material service life.
2. A key observation from this review is that carbonation encompasses both degradation and potential modification pathways. Under controlled conditions, carbonation reactions can contribute to CO_2 sequestration and certain performance improvements, though the practical realization of these benefits requires careful management of competing effects. Beneficial densification should be weighed against the risk of mi-

crocracking; rapid reaction kinetics must be balanced with uniform phase distribution to avoid deleterious gradients. Understanding C-S-H carbonation may offer contributions toward addressing climate change and infrastructure sustainability goals, consistent with broader circular economy objectives. Future developments will likely depend on combining multi-scale characterization with improved predictive modeling, developing admixtures that reduce carbonate crystallization, and establishing validation protocols for new materials and techniques.

3. Several limitations and unresolved questions remain. Real-time monitoring of silica gel structural evolution during carbonation presents ongoing experimental challenges. The progression from amorphous calcium carbonate through vaterite to calcite in confined nanoscale pores is not yet fully quantified. Perhaps most significantly, existing methods for predicting service-life carbonation depths from short-term laboratory data show considerable uncertainty, contributing to variability in field performance assessments. By assembling mechanisms, influencing factors, and mitigation approaches, this work aims to support researchers and practitioners in developing concrete structures with improved durability characteristics, advancing understanding of structure–property relationships in carbonated cementitious systems.

Author Contributions: Conceptualization, formal analysis, writing—original draft, writing—review and editing, supervision, investigation, and project administration, J.W.; formal analysis, writing—original draft, writing—review and editing, and investigation, Y.Z. All authors have read and agreed to the published version of the manuscript.

Funding: This research received no external funding.

Institutional Review Board Statement: Not applicable.

Informed Consent Statement: Not applicable.

Data Availability Statement: No new data were created or analyzed in this study.

Acknowledgments: The authors would like to thank Central South University and Beijing No. 4 Municipal Construction Engineering Co., Ltd., for their support.

Conflicts of Interest: Author Yi Zhao was employed by the company Beijing No. 4 Municipal Construction Engineering Co., Ltd. The remaining authors declare that the research was conducted in the absence of any commercial or financial relationships that could be construed as a potential conflict of interest.

References

1. Deng, G.; Zhang, N.; Liao, W.; He, Y.; Lu, L.; Chi, L.; Ma, H. Carbonated blast-furnace slag as supplementary cementitious material: Phase transition and effect on cement hydration. *Mater. Des.* **2026**, *261*, 115292. [CrossRef]
2. He, J.; Zhao, Y.; Tao, Y.; Shen, P.; Poon, C.S. Insights into the synergistic action of initial hydration and subsequent carbonation of Portland cement. *Cem. Concr. Compos.* **2025**, *157*, 105924. [CrossRef]
3. Xu, Y.; Liang, X.; Wan, C.; Yang, H.; Feng, X. Carbonation and related behaviors of hardened cement pastes under different hydration degrees. *Cem. Concr. Compos.* **2023**, *140*, 105079. [CrossRef]
4. Guo, Z.; Wang, Y.; Pei, T.; Wang, H. Cui, Effect of different hydration-carbonation processes on the reaction degree of cement. *Constr. Build. Mater.* **2024**, *451*, 138743. [CrossRef]
5. Zhan, B.J.; Xuan, D.X.; Poon, C.S.; Shi, C.J.; Kou, S.C. Characterization of C-S-H formed in coupled CO_2-water cured Portland cement pastes. *Mater. Struct.* **2018**, *51*, 92. [CrossRef]
6. Liu, X.; Feng, P.; Cai, Y.; Yu, X.; Liu, Q. Carbonation behaviors of calcium silicate hydrate (C-S-H): Effects of aluminum. *Constr. Build. Mater.* **2022**, *325*, 126825. [CrossRef]
7. Zeng, J.; Feng, D.; Liu, C.; Ye, G.; Ma, C.; Tian, J.; Mu, Y. Effect of ageing on the hydration and carbonation reactivity of ordinary Portland cement. *J. Build. Eng.* **2025**, *111*, 113598. [CrossRef]
8. Hu, X.; Xu, L.; Li, M.; Wang, J.; Ran, B.; Huang, R.; Zhou, X.; Xiong, Y. Effect of temperature and superplasticizer on hydration of C_3S and carbonation products of C-S-H. *Constr. Build. Mater.* **2024**, *444*, 137864. [CrossRef]

9. Ye, X.; Chen, T.; Chen, J. Carbonation of cement paste under different pressures. *Constr. Build. Mater.* **2023**, *370*, 130511. [CrossRef]
10. Wang, Y.; Tang, H.; Su, J.; He, H.; Zhao, Y.; Wang, J. Effect of sodium sulfate and gypsum on performances of expansive grouting material with aluminum as expansion agent. *Constr. Build. Mater.* **2023**, *394*, 132212. [CrossRef]
11. Wang, J.; Liu, E. The relationship between steady-state chloride diffusion and migration coefficients in cementitious materials. *Mag. Concr. Res.* **2020**, *72*, 1016–1026. [CrossRef]
12. He, H.; Wang, Y.; Wang, J. Effects of aggregate micro fines (AMF), aluminum sulfate and polypropylene fiber (PPF) on properties of machine-made sand concrete. *Appl. Sci.* **2019**, *9*, 2250. [CrossRef]
13. Xie, J.; Wang, J.; Li, M.; Xu, L.; Xiang, D.; Wang, Y.; He, H.; Zhu, Y.; Zhao, J. Estimation of chloride diffusion coefficient from water permeability test of cementitious materials. *Constr. Build. Mater.* **2022**, *340*, 127816. [CrossRef]
14. Li, J.; Zhang, W.; Ye, J.; Luo, K.; Ren, X.; Lu, Z. Mechanism of pore structure on carbonation properties of cement with high carbon fixation capacity. *Constr. Build. Mater.* **2025**, *462*, 139919. [CrossRef]
15. Savija, B.; Lukovic, M. Carbonation of cement paste: Understanding, challenges, and opportunities. *Constr. Build. Mater.* **2016**, *117*, 285–301. [CrossRef]
16. Chen, J.; Tang, L.; Yi, J.; Wu, K.; Zhang, J. Progress Analysis and Prospect on the Influence of Early-Age Carbonation Curing on Properties of Cement-Based Materials. *Processes* **2025**, *14*, 97. [CrossRef]
17. Auroy, M.; Poyet, S.; Le Bescop, P.; Torrenti, J.-M.; Charpentier, T.; Moskura, M.; Bourbon, X. Comparison between natural and accelerated carbonation (3% CO_2): Impact on mineralogy, microstructure, water retention and cracking. *Cem. Concr. Res.* **2018**, *109*, 64–80. [CrossRef]
18. Zheng, T.; Zhang, J.; Oh, D.; Kitagaki, R. The Initial Carbonation Behavior of Synthetic C-S-H by Relative Humidity. In Proceedings of the 4th FIB International Conference on Concrete Sustainability, Guimaraes, Portugal, 11–13 September 2024; pp. 359–365.
19. Teune, I.E.; Schollbach, K.; Florea, M.V.A.; Brouwers, H.J.H. Carbonation of hydrated cement: The impact of carbonation conditions on CO_2 sequestration, phase formation, and reactivity. *J. Build. Eng.* **2023**, *79*, 107785. [CrossRef]
20. Li, G.; Liu, S.; Hu, X.; Zhu, J.; Guan, X.; Shi, C. Effect of pH environment on carbonation properties of γ-C_2S. *Constr. Build. Mater.* **2025**, *461*, 139888. [CrossRef]
21. Gong, P.; Mei, K.; Zhang, L.; Xue, Q.; Wang, X.; Wei, T.; Zhang, C.; Cheng, X. Hydration and carbonation reaction dynamics in CO_2-rich environment for tricalcium silicate (C_3S) and dicalcium silicate (C_2S). *Powder Technol.* **2025**, *452*, 120535. [CrossRef]
22. Zajac, M.; Irbe, L.; Bullerjahn, F.; Hilbig, H.; Haha, M.B. Mechanisms of carbonation hydration hardening in Portland cements. *Cem. Concr. Res.* **2022**, *152*, 106687. [CrossRef]
23. Jiang, J.; Chen, X.; Li, L.; Yan, W.; Zhang, M.; Gang, Z.; Ma, Q.; He, J.; Dai, X. Performance of Cementitious Materials Subjected to Low CO_2 Concentration Accelerated Carbonation Curing and Further Hydration. *Buildings* **2026**, *16*, 187. [CrossRef]
24. Zajac, M.; Skibsted, J.; Skocek, J.; Durdzinski, P.; Bullerjahn, F.; Haha, M.B. Phase assemblage and microstructure of cement paste subjected to enforced, wet carbonation. *Cem. Concr. Res.* **2020**, *130*, 105990. [CrossRef]
25. Lippiatt, N.; Ling, T.-C.; Eggermont, S. Combining hydration and carbonation of cement using super-saturated aqueous CO_2 solution. *Constr. Build. Mater.* **2019**, *229*, 116825. [CrossRef]
26. Sun, H.; Luo, X.; Ren, Z.; Zhong, J.; Jin, Y.; Cui, H.; Wang, Y.; Hanein, T. Effect of carbonation curing on C_3S, C_2S, C_3A and C_4AF phases: Microstructure and reactivity mechanisms. *J. Build. Eng.* **2025**, *112*, 113819. [CrossRef]
27. Mehdizadeh, H.; Jia, X.; Mo, K.H.; Ling, T.-C. Effect of water-to-cement ratio induced hydration on the accelerated carbonation of cement pastes. *Environ. Pollut.* **2021**, *280*, 116914. [CrossRef]
28. Zhang, Z.; Zheng, K.; Song, H.; Chen, L.; Yuan, Q.; Cao, Q. Enhancing the Mechanism of Inert Fillers on Carbonation Properties of γ-Calcium Silicate Compacts. *ACS Sustain. Chem. Eng.* **2025**, *13*, 17103–17118. [CrossRef]
29. Zajac, M.; Skibsted, J.; Durdzinski, P.; Haha, M.B. Effect of alkalis on products of enforced carbonation of cement paste. *Constr. Build. Mater.* **2021**, *291*, 123203. [CrossRef]
30. Tuinukuafe, A.A.; Yoon, H.; Mills, M.M.; Mitchell, C.A.; Noell, P.J.; Rimsza, J.M. Effect of calcite filler on carbonation behavior in a synthesized C-S-H binder. *J. Am. Ceram. Soc.* **2025**, *109*, 70361. [CrossRef]
31. Yang, H.; Zhang, Y.; Ding, S.; Zhao, Q.; Chang, J.; Poon, C.S. Carbonation of ettringite and monosulfate: Product evolution, microstructure, and comparison. *Cem. Concr. Compos.* **2025**, *164*, 106297. [CrossRef]
32. Cai, Y.; Feng, P.; Liu, X.; Shen, X.; Lothenbach, B. Simultaneous formation and decomposition of calcium silicate hydrate under carbonation in water. *Cem. Concr. Res.* **2026**, *199*, 108021. [CrossRef]
33. Zheng, H.; Duan, Y.; Lu, X.; Li, M.; Chen, J.; Jin, Z.; Hou, D.; Hong, S.; Wang, P.; Dong, B. Molecular-scale insights into the leaching of Ca ions and carbonate deposition behavior in CSH under carbonation. *J. Build. Eng.* **2024**, *98*, 111358. [CrossRef]
34. Black, L.; Breen, C.; Yarwood, J.; Garbev, K.; Stemmermann, P.; Gasharova, B. Structural features of C-S-H(I) and its carbonation in air—A Raman spectroscopic study. Part II: Carbonated phases. *J. Am. Ceram. Soc.* **2007**, *90*, 908–917. [CrossRef]
35. Li, L.; Liu, Q.; Dao, V.; Wu, M. Dimensional change of cement paste subjected to carbonation in CO_2 sequestration and utilization context: A critical review on the mechanisms. *J. CO_2 Util.* **2023**, *70*, 102444. [CrossRef]

36. Ren, M.; Shen, P.; Tao, Y.; Poon, C.-S. Development of highly carbonation-effective calcium silicates (β-C_2S): Phase evolution, microstructure, and carbonation mechanisms. *Cem. Concr. Res.* **2024**, *181*, 107542. [CrossRef]
37. Chen, W.; Xu, W.; Li, Y. Microstructural Investigation of Carbonation of Calcium Silicate Hydrate in Hydrated Cement Paste. In Proceedings of the International Conference on Civil Engineering and Building Materials (CEBM), Kunming, China, 26–28 July 2011; pp. 601–605.
38. Wang, J.; Xu, H.; Xu, D.; Du, P.; Zhou, Z.; Yuan, L.; Cheng, X. Accelerated carbonation of hardened cement pastes: Influence of porosity. *Constr. Build. Mater.* **2019**, *225*, 159–169. [CrossRef]
39. Li, B.; Ma, Y.; He, J.; Mu, S.; Zhao, H.; Zhuang, Z.; Li, W.; Yang, H.; Zhang, Z.; Gu, Q.; et al. Wet carbonation of calcium silicate hydrate (C-S-H): Structural transformation and calcium carbonate crystallization pathways. *J. Build. Eng.* **2025**, *113*, 114090. [CrossRef]
40. Huang, R.; Xu, L.; Cai, Y.; Ran, B.; Wang, J. Investigations on the hydration of C_3S with different water–solid ratios and subsequent carbonation. *Mag. Concr. Res.* **2025**, *77*, 434–447. [CrossRef]
41. Cui, K.; Zheng, Y.; Zhao, Y.; Qin, Q.; Liang, K.; Chang, J.; Liu, F.; Shen, P.; Poon, C.S. Development of in-situ highly active calcium carbonate through anhydrous carbonation of OPC: Effect on hydration and properties of cement composites. *Cem. Concr. Res.* **2025**, *197*, 107980. [CrossRef]
42. Wang, Y.; Chen, F.; Li, Z.; Yang, W.; Zhan, B.; Li, D.; Xing, F.; Li, W. Mechanism Analysis on Carbonation of Hardened Cement Paste with XCT. *J. Mater. Civ. Eng.* **2023**, *35*, 04023323. [CrossRef]
43. Wang, Z.; Zhou, H.; Lian, S.; Meng, T.; Yu, H.; Zhou, X.; Wang, S.; Ruan, S. Hydration behaviors, workability, and strength variations in direct aqueous carbonation (DAC) of Portland cement paste. *Sci. Rep.* **2025**, *15*, 5517. [CrossRef] [PubMed]
44. Kopitha, K.; Krishnya, S.; Elakneswaran, Y.; Kitagaki, R.; Yoda, Y.; Tsujino, M.; Nishida, A. Effect of Carbonation on Microstructure of Cement Pastes with Different Water-to-Cement Ratios. In *ICSBE 2022: Proceedings of the 13th International Conference on Sustainable Built Environment*; Lecture Notes in Civil Engineering; Springer: Singapore, 2023; Volume 362, pp. 149–159.
45. Shen, Q.; Pan, G.; Bao, B. Influence of CSH carbonation on the porosity of cement paste. *Mag. Concr. Res.* **2016**, *68*, 504–514. [CrossRef]
46. Zhang, Z.; Liu, Z.; Wang, F.; Hu, S.; Feng, P. New Insights into the Carbonation Behavior of C_3S_2: Elucidating the Role of Silica Gel in the Mechanical Strength of Carbonated Matrix. *ACS Sustain. Chem. Eng.* **2025**, *13*, 13261–13273. [CrossRef]
47. Hu, L.; Jia, Y.; Chen, Z.; Yao, Y.; Sun, J.; Xie, Q.; Yang, H. An insight of carbonation-hydration kinetics and microstructure characterization of cement paste under accelerated carbonation at early age. *Cem. Concr. Compos.* **2022**, *134*, 104763. [CrossRef]
48. Guan, Q.; Ma, Y.; Liu, Z.; He, J.; Wang, Z.; Zhao, H.; Jin, M.; Liu, J. Investigation of synergistic reactions and microstructural changes in Belite-rich cement under early carbonation followed by hydration. *Constr. Build. Mater.* **2025**, *490*, 142506. [CrossRef]
49. Du, H.; Liu, W.; Long, G. Microstructure and water absorption of chloride-containing hardened cement pastes under accelerated carbonation condition. *Constr. Build. Mater.* **2025**, *463*, 140106. [CrossRef]
50. Liang, C.; Li, B.; Guo, M.-Z.; Hou, S.; Wang, S.; Gao, Y.; Wang, X. Effects of early-age carbonation curing on the properties of cement-based materials: A review. *J. Build. Eng.* **2024**, *84*, 108495. [CrossRef]
51. Rostami, V.; Shao, Y.; Boyd, A.J.; He, Z. Microstructure of cement paste subject to early carbonation curing. *Cem. Concr. Res.* **2012**, *42*, 186–193. [CrossRef]
52. Chen, T.; Gao, X. Effect of carbonation curing regime on strength and microstructure of Portland cement paste. *J. CO_2 Util.* **2019**, *34*, 74–86. [CrossRef]
53. Adem, J.K.; Seo, J.; Park, S.; Kim, G.M. Effects of low-lime calcium silicate cement addition on the hydration, carbonation, and microstructural characteristics of OPC pastes by carbonation curing. *J. Build. Eng.* **2025**, *107*, 112683. [CrossRef]
54. Tang, Y.; Yu, K.; He, C.; Gao, L.; Yang, H.; He, H.; Zhong, A.-N. Research progress on the application of low-reactivity minerals in carbonation-cured cement-based materials. *J. CO_2 Util.* **2024**, *88*, 102938. [CrossRef]
55. Bersisa, A.; Moon, K.-Y.; Kim, G.M.; Cho, J.-S.; Park, S. Influence of hydraulic cement substitutes on carbonation of calcium silicate cement. *Constr. Build. Mater.* **2025**, *473*, 140800. [CrossRef]
56. Xia, J.; Li, C.; Ma, H.; Ren, Q. Mix Design-Driven Control of Carbonation and Hydration in CO_2-Mixed Cement Pastes: Effects of Water, Slag, and Surfactant. *Buildings* **2025**, *15*, 2116. [CrossRef]
57. Wang, H.; Gu, X.; Liu, J.; Zhu, Z.; Wang, S.; Xu, X.; Nehdi, M.L. Synergistic effects of steel slag and lithium slag in carbonation-cured cement pastes: Carbonation degree, strength and microstructure. *J. Build. Eng.* **2024**, *85*, 108706. [CrossRef]
58. Gong, Y.; Song, Z.; Liu, B.; Sun, G.; Sun, G.; Chen, H. Improving the carbonation resistance of supersulfated cement with γ-C_2S. *J. Build. Eng.* **2026**, *118*, 114998. [CrossRef]
59. Xu, L.; Wang, J.; Huang, R.; Wang, Y.; Ran, B.; Hu, X.; Lv, T.; Zhou, X.; Wang, S.; Dai, X. Effects of accelerated carbonation on the chemical and microstructural evolution of recycled different SCMs blended cement pastes. *Cem. Concr. Compos.* **2025**, *164*, 106259. [CrossRef]

60. Wang, Y.; Tian, Y.; Wang, J. Effects of carbide slag and CO_2 curing on physical properties of gypsum plaster. *ACI Mater. J.* **2020**, *117*, 170–178. [CrossRef]
61. Wang, J. Effective Coating System Should Be Applied to Concrete with Recycled Waste Materials. *Coatings* **2022**, *12*, 1133. [CrossRef]